Complex permittivities of a nematic liquid crystal in a hybrid-aligned cell

Fuzi Yang

Department of Chemistry, Tsinghua University, Beijing 100084, China

S. A. Jewell, Lizhen Ruan, and J. R. Sambles

Thin Film Photonics, School of Physics, University of Exeter, Stocker Road, Exeter EX4 4QL, United Kingdom

Received August 18, 2006; revised November 3, 2006; accepted November 8, 2006;
posted November 13, 2006 (Doc. ID 74186); published February 15, 2007

The half-leaky guided-mode (HLGM) technique has been used to explore a hybrid-aligned nematic (HAN) liquid-crystal cell. With a suitably oriented cell the optical response of the system, as a function of incident angle, has some unusual features. It is found that beyond a particular angle of incidence, with light incident from the homeotropically aligned side, the apparent mode spacing increases with increasing angle, which is entirely opposite to that found for an isotropic slab of material. This clearly indicates that the effective cell thickness varies with incident angles, an effect caused by the director profile within the cell, leading to bent trajectories for the beams propagating inside the cell. For this situation the depths of the reflectivity minima associated with excitation of the waveguide modes are particularly sensitive to the imaginary parts of the permittivities of the liquid crystal. This has enabled the two imaginary parts of the parallel and perpendicular permittivities of the liquid crystals to be determined separately. The technique is a very useful and accurate method for determining the whole optical tensor of the liquid crystal.

OCIS codes: 160.3710, 310.2790.

1. INTRODUCTION

Recently the hybrid-aligned nematic (HAN) liquid-crystal cell geometry has received substantial attention both from a fundamental physics perspective and in regard to potential applications. This is partly because a HAN cell has no threshold voltage, partly because it resembles some of the bistable structures being developed, and partly because this geometry may also lead to interesting and useful optical responses. Using a HAN-cell configuration the flexoelectric effect and dual-frequency materials[1–3] have been investigated. Others have explored the nature of the optical beam trajectory inside a HAN cell and its potential use in devices.[4,5] If *p*-polarized light is incident on the homeotropically aligned face of a HAN cell in which the director is untwisted and lies completely within the plane of incidence, then the cell acts as a waveguide of varying effective thickness, with thickness dependent upon the optical incident angle. This behavior will manifest itself in angle-dependent reflectivity spectra and may be fully explored using optical waveguide techniques.

In this study the half-leaky guided-mode (HLGM) technique[6] has been used to explore a HAN cell in detail. This allows for the determination of the full optical tensor (real and imaginary components) and the director profile and gives great insight into the form of the optical field distribution within the cell. From analysis of the guided-mode distribution as a function of incident angle, we find that beyond a special critical angle the mode spacing of the *p*-polarized reflectivity R_{PP} (for the director lying in the plane of incidence, Euler twist angle of 90°) increases with increasing angle. This is entirely opposite to the behavior of a normal waveguide.[7] This clearly indicates that the effective waveguide thickness varies with incident angle and shows the nature of the bent trajectory of the beam propagating inside the cell.[5] This is then confirmed by direct experimentation. In addition it is found that the depths of the reflectivity minima associated with excitation of the waveguide modes are particularly sensitive to the imaginary parts of the optical permittivities of the liquid-crystal material. Further while in one angle region the depths are dictated by one imaginary component, in a separate angle region the other dominates, thereby allowing the determination of both these parameters. Thus this technique is a very useful and accurate method for determining the whole optical tensor of the liquid-crystal material, which is not achievable with any other optical techniques such as ellipsometry.

2. ANALYSIS

The HLGM geometry of the HAN cell is shown in Fig. 1(a) with $n_1 > n_e > n_o > n_2$. It is clear that there are three different critical angles available within this system. The first, at an angle β_{C1}, corresponds to the critical angle between the top high-index pyramid (n_1) and the bottom low-index glass plate (n_2), i.e., $\beta_{C1} = \sin^{-1}(n_2/n_1)$. The second, at an angle β_{C2}, corresponds to the critical angle between the high-index pyramid (n_1) and the ordinary liquid-crystal index (n_o), i.e., $\beta_{C2} = \sin^{-1}(n_o/n_1)$. The third, at an angle, β_{C3}, corresponds to the critical angle between

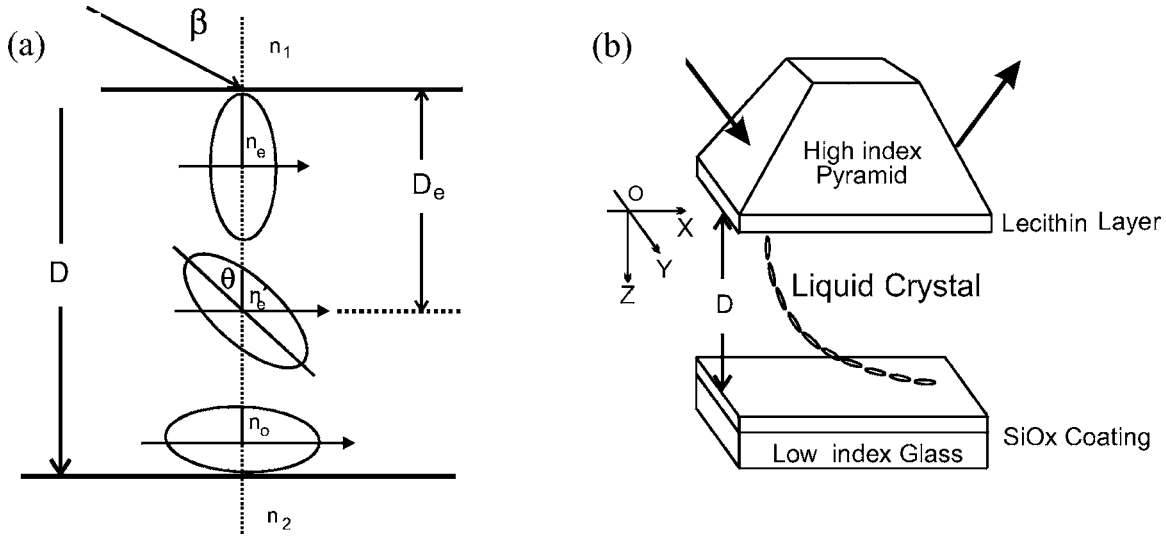

Fig. 1. (a) HAN cell geometry; (b) HLGM experimental arrangement.

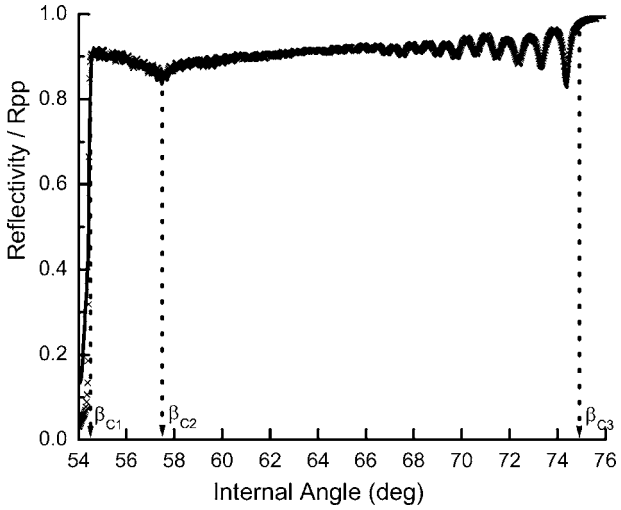

Fig. 2. Experimentally recorded in-plane reflectivity data, R_{pp} (x's) and theoretical fit (solid curve) for a HAN cell.

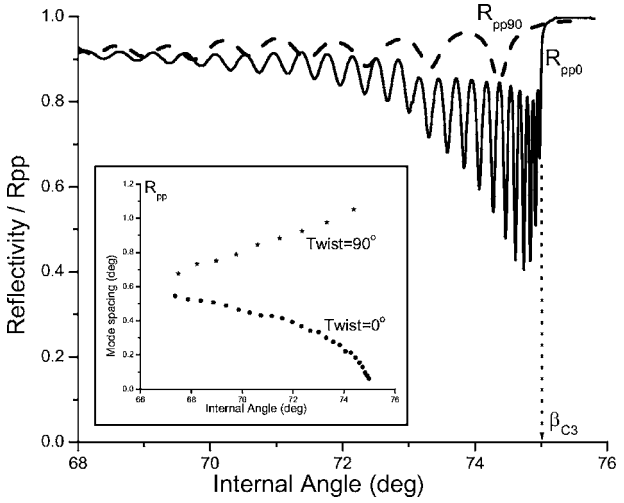

Fig. 3. Experimentally recorded in-plane and out-of-plane reflectivity data for a HAN cell for higher angles of incidence. (Inset, mode spacing against mode position for both in-plane and out-of-plane cases for a HAN cell over the higher incident angles.)

the high-index pyramid (n_1) and the extraordinary index of the liquid crystal (n_e), i.e., $\beta_{C3}=\sin^{-1}(n_e/n_1)$. From this it is clear that for incident angles $\beta<\beta_{C1}$, the optical beam will propagate through the entire cell into the bottom glass plate, while conversely for incident angles $\beta>\beta_{C3}$, the beam will be totally reflected at the pyramid–liquid-crystal interface and only an evanescent field near the pyramid–liquid-crystal interface penetrates into the liquid-crystal layer. Then, because of the HAN structure, the optical field propagation depth will gradually reduce from D, the whole thickness of the liquid crystal, to zero on increasing β_e from β_{C1} to β_{C3}. From Snell's law we have

$$n_1 \sin \beta_e = n_e', \tag{1}$$

where

$$n_e' = \frac{n_o n_e}{\sqrt{{n_e}^2 \sin^2 \theta(D_e) + {n_o}^2 \cos^2 \theta(D_e)}}, \tag{2}$$

in which D_e is the depth at which the incident field is totally internally reflected. Then if, for simplicity, one assumes a linear variation of the director tilt across the HAN cell:

$${n_1}^2 \sin^2 \beta_e = \frac{{n_e}^2}{1+[({n_e}^2-{n_o}^2)/{n_o}^2]\sin^2(\pi D_e/2D)}, \tag{3}$$

there is a simple relationship between $1/\sin^2\beta_e$ and $\sin^2(\pi D_e/2D)$ of the form

$$\frac{1}{\sin^2 \beta_e} = \frac{n_1^2}{n_e^2} + \left(\frac{n_1^2}{n_o^2} - \frac{n_1^2}{n_e^2}\right)\sin^2\left(\frac{\pi D_e}{2D}\right). \tag{4}$$

3. EXPERIMENT

The sample geometry for the experimental measurements is shown in Fig. 1(b). Incident light is provided by a He–Ne laser (632.8 nm) sent into the cell p polarized and

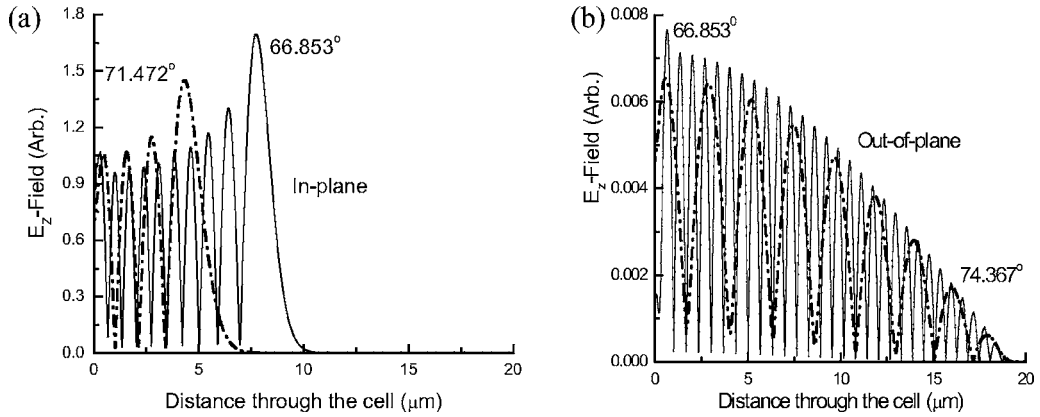

Fig. 4. (a). Modulus of the optical E_Z-field distribution through the HAN cell for two different incident angles for the in-plane case. (b) Modulus of the optical E_Z-field distribution through the HAN cell for two different incident angles for the out-of-plane case. Arb., arbitrary units.

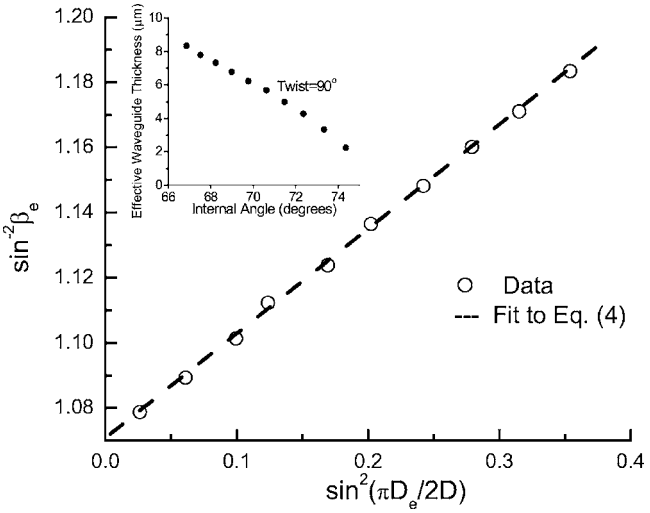

Fig. 5. Plot of $\sin^2(\pi D_e/2D)$ against $\sin^2\beta$ of a HAN cell for the in-plane situation. (Inset, effective thickness of a HAN cell waveguide against the angular mode position for the in-plane situation.)

modulated so that by using phase-sensitive detectors, a good signal-to-noise ratio is achieved. The cell boundaries are provided by a high-index pyramid (for coupling in light) with a permittivity of 3.2400 and a low-index glass plate with a permittivity of 2.1460 for 632.8 nm radiation. To form the requisite HAN geometry, a lecithin monolayer is deposited from ether solution on the pyramid's bottom surface to give the needed homeotropic alignment, while a 60° evaporated SiOx thin coating on the glass plate gives homogeneous alignment. Two mylar strips of about 18 μm thickness are used as cell spacers. Then this arrangement is capillary filled with the nematic liquid-crystal material (E7-Merck-BDH) at room temperature. This whole sample geometry is placed into a rotatable frame on a computer-controlled rotating table. Angle-dependent reflectivity signals, R_{pp}, are recorded, one for the director in the plane of incidence (in plane) and one with the cell rotated by 90° with the director normal to the incident plane (out of plane).

The R_{pp} data recorded for the case of the director profile lying in the incident plane (in plane, Euler twist angle of 90°) are shown in Fig. 2 as x's. The three critical angles mentioned in the analysis above are clearly indicated in this figure. To allow a comparison of the mode spacings at higher incident angles, data were also taken with the sample rotated by 90° (out of plane, Euler twist angle of 0°). Both sets of experimental data, for the high-angle range are shown in Fig. 4; very different mode spacings are apparent.

4. DISCUSSION

Using a scattering-matrix version of multilayer optics theory[8] produces the solid-curve fit to the data as shown in Fig. 2. The fit was chosen to be optimum above β_{C1}, with the data below this point ignored during the fitting procedure but included in the plot for reference. The parameters for this fitting are $\epsilon_{\|}=3.0285$ (±0.0005) $+i\ 0.00022(\pm0.00002)$, $\epsilon_{\perp}=2.3050$ (±0.0005)$+i0.00013$ (±0.00002), and $D=19.10$ μm for the liquid crystal, E7; $\epsilon_S=2.5510$ and $D_S=25$ nm for the SiOx thin coating. The fit of the theoretical prediction (solid curve) to the experimental results (x's) is excellent but not perfect; this slight misfit is probably caused by the quality of the SiOx layer. The influence of ϵ_i is discussed in detail later.

From Fig. 3 the mode minima positions in terms of incident angles and their spacings are readily determined. These are plotted in the inset in Fig. 3 as the mean mode spacing between adjacent minima against the mode position for the two experimentally recorded reflection signals. It is clear that for the in-plane reflectivity, the mode spacing increases with increase of incident angle, which is entirely opposite to the data for the out-of-plane reflectivity, the normal behavior for a waveguide with constant thickness. This means that for the in-plane situation the effective thickness of the cell must be varying (decreasing) with increasing incident angle. From the multilayer optical fit to the data, some optical E_Z-field distributions through the cell have been modeled for both low and high incident angles for both in-plane and out-of-plane situations. These optical field models are shown in Fig. 4(a) and 4(b), respectively. For the interesting in-plane case the higher the incident angle, the lower the effective thickness, while for the out-of-plane case the waveguide thickness is independent of the incident angle.

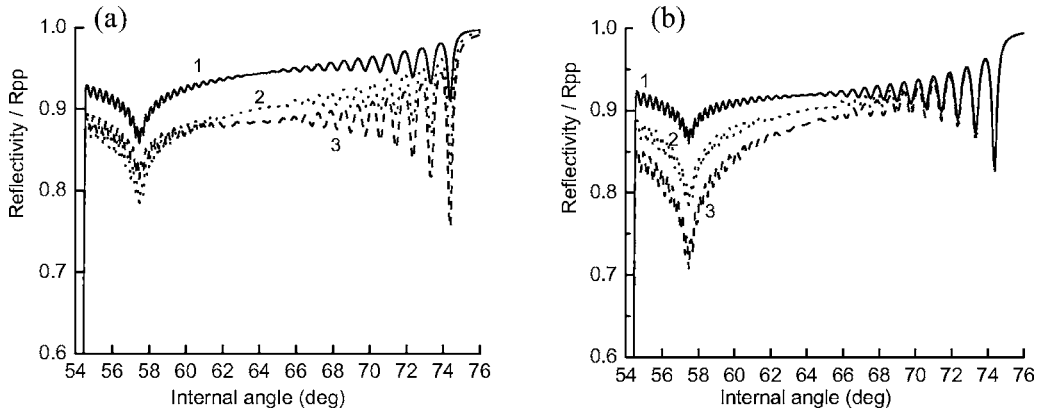

Fig. 6. (a) Influence of three different imaginary parts of the perpendicular permittivity of the liquid crystal for the in-plane case: (1) $\epsilon_i=0.0001$, (2) $\epsilon_i=0.0002$, (3) $\epsilon_i=0.0003$. (b) Effects of the three different imaginary parts of the parallel permittivity of the liquid crystal for the in-plane case: (1) $\epsilon_i=0.0001$, (2) $\epsilon_i=0.0002$, (3) $\epsilon_i=0.0003$.

An effective thickness D_e is defined (somewhat arbitrarily) as the measured distance from the input surface to the last maximum in the oscillating electric-field profile in plots such as Fig. 4(a). The plot of D_e against mode angle β_e is presented in the inset in Fig. 5. From this we may produce a graph of $1/\sin^2\beta_e$ against $\sin^2(\pi D_e/2D)$, giving the simple linear relationship shown in Fig. 5. From the slope and intercept with the vertical axis of the straight-line fit, $n_e/n_o=1.145\pm0.001$, which is in accord with the expected value of 1.146.

From Fig. 2 it is apparent that between β_{C1} and β_{C2} the overall level of the reflectivity gradually decreases and that between β_{C2} and β_{C3} the overall level increases with incident angle. This effect is associated with absorption by the liquid crystal. Between β_{C1} and β_{C2} the waveguide thickness is constant, and so for increasing incident angle the light travels farther through the liquid-crystal layer, thereby increasing the loss. However from β_{C2} to β_{C3} the effective thickness of the waveguide decreases as the incident angle increases, and the absorption thus decreases. The reflectivity data are thereby quite sensitive to absorption by the liquid-crystal layer and hence to the imaginary parts of the liquid-crystal permittivities.

The influence of the imaginary part of the liquid-crystal optical permittivity is modeled and shown in Figs. 6(a) and 6(b). In Fig. 6(a) the imaginary part of $\epsilon_\perp$ is taken as 0.0001, 0.0002, and 0.0003 for curves 1, 2, and 3, respectively, while $\epsilon_\parallel$ is held at 0.0001. In Fig. 6(b) the imaginary part of $\epsilon_\parallel$ is taken as 0.0001, 0.0002, and 0.0003 for curves 1, 2, and 3, respectively, while $\epsilon_\perp$ is held at 0.0001. It is obvious that the reflection signals are very sensitive to the imaginary part of the liquid-crystal permittivity and that the separate influences of $\epsilon_\parallel$ and $\epsilon_\perp$ can be easily distinguished. Modeling suggests that this technique can be used to determine values of the imaginary part of the liquid-crystal optical permittivities up to $\sim$0.01 (above this point the optical signal is too small for any meaningful information to be obtained). Thus the HLGM technique for the HAN cell can be used to accurately determine the whole permittivity of the liquid crystal in the cell. In this study we find the imaginary parts of the parallel and perpendicular permittivities for E7, at room temperature, to be 0.00022 (±0.00002) and 0.00013 (±0.00002), respectively.

5. CONCLUSIONS

The HLGM technique has been used to characterize the director profile of HAN liquid-crystal cell. From the in-plane reflectivity data, R_{pp}, the nature of the cell, a waveguide with an effective thickness that varies with incident angle, has been clearly confirmed by our experiment. Modeling shows how the optical field, entering from the homeotropic side, penetrates to different depths of the cell, before being totally internally reflected, as the angle of incidence is varied. The behavior of the mode spacing with incidence angle confirms the analytic theory, while a detailed comparison between multilayer optical scattering theory and the data fully confirms the expected director profile.

In addition the influence of the imaginary components of the optical permittivity tensor are found to be significant and different from the two components of the uniaxial permittivity. As a result, this technique has been used to determine the complete uniaxial permittivity tensor, including the imaginary parts, for the liquid-crystal material.

ACKNOWLEDGMENT

The authors gratefully acknowledge financial support from the Royal Society for this British–Chinese cooperative project.

Corresponding author S. A. Jewell can be reached by e-mail at s.a.jewell@exeter.ac.uk.

REFERENCES

1. S. A. Jewell and J. R. Sambles, "Fully-leaky guided mode measurement of surface polarization in a HAN liquid crystal cell," J. Appl. Phys. **92**, 19–24 (2002).
2. S. A. Jewell and J. R. Sambles, "Backflow in the relaxation of a hybrid aligned nematic cell," Appl. Phys. Lett. **82**, 3156–3158 (2003).
3. S. A. Jewell and J. R. Sambles, "Optical characterization of a dual-frequency hybrid aligned nematic liquid crystal cell," Opt. Express **13**, 2627–2633 (2005).
4. J. A. Olivares, R. F. Rodriguez, and J. A. Reyes, "Ray tracing and reflectivity measurements in nematic hybrid cells," Opt. Commun. **221**, 223–239 (2003).
5. C. I. Mendoza, J. A. Olivares, and J. A. Reyes, "Electrically

controlled total internal reflection in nematic hybrid cells," Phys. Rev. E **70**, 062701 (2004).
6. F. Yang and J. R. Sambles, "The optical tensor configuration in a surface stabilized ferroelectric liquid crystal determined by using half leaky guided modes," Liq. Cryst. **13**, 1–13 (1993).
7. A. W. Snyder and J. D. Love, *Optical Waveguide Theory* (Kluwer Academic, 1983).
8. D. Y. K. Ko and J. R. Sambles, "Scattering matrix method for propagation of radiation in stratified media: attenuated total reflection studies of liquid crystals," J. Opt. Soc. Am. A **5**, 1863–1866 (1988).